Computational Fluid Dynamics JOURNAL vol.1 no.4 January 1993 (429 — 442)

NUMERICAL ANALYSIS OF THREE DIMENSIONAL FLOW IN AN ELLIPTICAL DUCT BY REYNOLDS STRESS MODEL AND BOUNDARY-FITTED COORDINATE SYSTEM

Hitoshi SUGIYAMA † Mitsunobu AKIYAMA † Nao NINOMIYA †
Masaru HIRATA ‡ Kenichi SAITOH †

Abstract

The three dimensional Navier-Stokes equations and the Reynolds stress equation were solved for turbulent flows in an elliptical duct with an aspect ratio of 2:1. The calculation was carried out by using the Reynolds stress model on a boundary-fitted coordinate system. The calculated friction coefficients and mean flow velocity distributions were compared with published experimental data. The present method is able to predict the secondary flow of the second kind which is characteristic to the anisotropic turbulent flows. These calculated results clearly explain the anisotropy of normal stresses in an elliptical duct and suggest that the present method can predict the three dimensional turbulent flow in non circular ducts.

1. INTRODUCTION

The three dimensional turbulent flows in ducts or passages with non-circular cross section are often encountered in engineering practice. Examples are flows in heat exchangers, turbomachinery, nuclear power reactors, air-conditioning systems, open channels and rivers, etc. For compact heat exchangers, it is often necessary to design the flow passages as non circular cross section in order to achieve the required heat transfer area and to ensure the minimum pressure drop within the given space limitation.

The flow in such duct is often accompanied by the secondary flow of the second kind which is induced by anisotropic turbulence. Although this secondary velocity is only of the order of two or three percent of the streamwise bulk velocity, its presence displaces the lines of constant axial velocity considerably toward the corners of the duct, and results in a relatively high velocity field there. Furthermore this secondary motion induces an increase of the wall shear stress towards corners. In open channel flows, the secondary flow of the second kind transports fluid with relatively low streamwise momentum towards the center portion of the channel and decreases the velocity maximum below the surface.

Therefore, the turbulent flow in non-circular ducts has motivated numerous research works since very beginning of the modern fluid dynamics [1]. The fully developed turbulent flows in a square duct has been most extensively studied experimentally [2, 3] as well as analytically [4, 5]. The rectangular ducts have been examined by Tracy [6] and Leutheusser [7]. Although most of these non-circular ducts have square or rectangular sections, Aly, Trupp and Gerrard

Presented at the 5th Numerical Fluid Dynamics Symposium – Tokyo on December 19 –21, 1991.
Received on February 10, 1992.

† Dept. Mechanical Systems Engineering, Utsunomiya University; Ishii-cho 2753, Utsunomiya 321, Japan
‡ Dept. Mechanical Engineering, University of Tokyo; Hongo 7-3-1, Bunkyo-Ku, Tokyo 113, Japan

[8] performed both experimental and analytical studies on the fully developed turbulent flow in a duct with an equilateral triangular section. Cain and Duffy [9] have measured the friction coefficient and the mean flow velocity, not the Reynolds stress though, for fully developed turbulent flow in elliptical ducts with the aspect ratio of 1.5:1 or 2:1. Gosman and Rapley [10] have numerically simulated the fully developed turbulent flows in an elliptical duct of the aspect ratio 2:1. Tatsumi and Yoshimura also reported numerical simulation results [11].

The authors have applied the Reynolds stress model to the numerical analysis of the flow in ducts with the square [12] and triangular [13] cross sections. Contrary to those ducts which have the corner regions, there is no such region in an elliptical duct. Therefore, it is interesting to study the generation of secondary flow of the second kind and the distributions of the Reynolds stresses. In addition, most of the previous numerical analysis assumed the fully developed turbulent flows, and few works are available concerning the entrance region. There is no information on detailed measurements of the Reynolds stresses. Therefore, the purpose of the present research is to analyze the developing turbulent flow in an elliptical duct by means of an anisotropic turbulence model and of a boundary-fitted coordinate system.

2. TECHNIQUE OF ANALYSIS

The anisotropic nature of the turbulence is expressed by the Reynolds stress equations. Nevertheless, an exact analysis of these equations is not yet available so that some kinds of modelings are required. A set of the differential equations governing transport of the Reynolds stresses is derived from the Navier-Stokes equation, namely:

$$\begin{aligned}\frac{\mathrm{D}\overline{u_iu_j}}{\mathrm{D}t} = &-\left[\overline{u_iu_k}\frac{\partial U_j}{\partial x_k}+\overline{u_ju_k}\frac{\partial U_i}{\partial x_k}\right]+\overline{\frac{p}{\rho}\left(\frac{\partial u_i}{\partial x_j}+\frac{\partial u_j}{\partial x_i}\right)}\\ &-\frac{\partial}{\partial x_k}\left[\overline{u_iu_ju_k}-\nu\frac{\partial\overline{u_iu_j}}{\partial x_k}-\overline{\frac{p}{\rho}\left(\delta_{jk}u_i+\delta_{ik}u_j\right)}\right]-2\nu\overline{\frac{\partial u_i}{\partial x_k}\frac{\partial u_j}{\partial x_k}}.\end{aligned} \tag{1}$$

The first term of the right hand side is the production term P_{ij}, the second term is the pressure strain correlation π_{ij}, the third term is the diffusion term, and the fourth term is the dissipation term ε_{ij}. Since it is difficult to obtain the solution of this Reynolds stress equation, it is necessary to introduce a model for the correlations appearing in it. For modeling of the convective and diffusion terms, the approximation by Rodi [14] was employed, in which these terms are expressed as a differential form of the Reynolds stress component, and it is transformed into an algebraic equation. In such Reynolds stress model equation, a particularly problematic task is to model the pressure - strain correlation term, which is also defined as the redistribution term. Following Chou [15], this can be expressed as follows:

$$\overline{\frac{p}{\rho}\frac{\partial u_i}{\partial x_j}}=\frac{1}{4\pi}\int_{\mathrm{vol}}\left[\overline{\left(\frac{\partial^2u_\ell u_m}{\partial x_\ell\partial x_m}\right)'\frac{\partial u_i}{\partial x_j}}+2\left(\frac{\partial U_\ell}{\partial x_m}\right)'\overline{\left(\frac{\partial u_m}{\partial x_\ell}\right)'\left(\frac{\partial u_i}{\partial x_j}\right)}\right]\frac{\mathrm{dvol}}{|x-y|}+S_{ij}, \tag{2}$$

where the terms with and without the prime correspond to the values at y and x, respectively. The first and second terms of the right hand side of (2) relate to the interactions of the fluctuating velocity correlations with the fluctuating velocities and with the mean strain, respectively. The term S_{ij} represents the wall effect. In the present model, we adopted the Rotta's linear return-to-isotropy model to the first term of the right hand side of (2), in which $\pi_{ij,1}$ is written

as:

$$(\pi_{ij,1} + \pi_{ji,1}) = -c_1 \frac{\varepsilon}{k} \left(\overline{u_i u_j} - \frac{2}{3} k \delta_{ij} \right), \tag{3}$$

where k and ε are the time-averaged, turbulence kinetic energy and energy dissipation rate, respectively. And c_1 represents an empirical constant.

For $\pi_{ij,2}$ the correlation can be approximated in the form:

$$\pi_{ij,2} = \left(\frac{\partial U_\ell}{\partial x_m} \right) a_{\ell j}^{mi}, \tag{4}$$

and a_{lj}^{mi} is the fourth order tensor, which is determined by the following kinematic constraints.

$$a_{lj}^{mi} = a_{lj}^{im} = a_{jl}^{im}, \tag{5}$$

$$a_{li}^{mi} \frac{\partial U_\ell}{\partial x_m} = 0, \tag{6}$$

$$a_{jj}^{mi} = 2\overline{u_m u_i}. \tag{7}$$

These constraints are different from Rotta's proposal constraints with respect to the form of (6). We adopted the above constraints for the reason that $\pi_{ij,2}$ is defined as the product of the fourth order tensor with the mean strain as seen in (4). The constraints (5), (6) and (7) arise from the symmetricity, the mass conservation and Green's theorem, respectively. The form of (7) suggests that the fourth order tensor might be approximated by linear combination of Reynolds stresses. The most general such tensor satisfying the symmetry constraints implied by (7) is written as

$$\begin{aligned} a_{lj}^{mi} = {} & \alpha \delta_{\ell j} \overline{u_m u_i} + \beta \left(\delta_{ml} \overline{u_i u_j} + \delta_{mj} \overline{u_i u_l} + \delta_{il} \overline{u_m u_j} + \delta_{ij} \overline{u_m u_l} \right) \\ & + c_2 \delta_{mi} \overline{u_l u_j} + \left\{ \eta \delta_{mi} \delta_{lj} + \nu \left(\delta_{ml} \delta_{ij} + \delta_{mj} \delta_{il} \right) \right\} k, \end{aligned} \tag{8}$$

which is introduced by Launder, Reece, and Rodi [16]. Here δ_{ij} represents the Kronecker delta and c_2, α, β, η, ν are the empirical constants. The application of (6) and (7) enables two constants of (8) to be expressed in terms of c_2. On combining (4) and (8), the complete influence of the mean strain on the pressure-strain correlation may be expressed in the following form.

$$\begin{aligned} (\pi_{ij,2} + \pi_{ji,2}) = {} & -(\alpha + \beta) \left(P_{ij} - \frac{2}{3} P_k \delta_{ij} \right) + \zeta \left(\frac{\partial U_i}{\partial x_j} + \frac{\partial U_j}{\partial x_i} \right) k \\ & + (4\beta + \alpha) \left(D_{ij} - \frac{2}{3} P_k \delta_{ij} \right), \end{aligned} \tag{9}$$

where

$$D_{ij} = -\overline{u_i u_k} \frac{\partial U_k}{\partial x_j} - \overline{u_j u_k} \frac{\partial U_k}{\partial x_i},$$

$$\alpha = \frac{1}{11} (4c_2 + 10), \quad \beta = -\frac{1}{11} (2 + 3c_2), \quad \zeta = \eta + \nu.$$

Table 1: Modeling of the pressure-strain correlation term

$\pi_{ij,1}+\pi_{ji,1}$	$-c_1\frac{\varepsilon}{k}\left(\overline{u_iu_j}-\frac{2}{3}k\delta_{ij}\right)$
$\pi_{ij,2}+\pi_{ji,2}$	$-\frac{c_2-8}{11}\left(P_{ij}-\frac{2}{3}P_k\delta_{ij}\right)+\zeta k\left(\frac{\partial U_i}{\partial x_j}+\frac{\partial U_j}{\partial x_i}\right)-\frac{8c_2-2}{11}\left(D_{ij}-\frac{2}{3}P_k\delta_{ij}\right)$
$[\pi_{ij}+\pi_{ji}]_w$	$c_1=c_1^*+c_1'f(\frac{L}{X_w}),\quad c_2=c_2^*+c_2'f(\frac{L}{X_w}),\quad \zeta=\zeta^*+\zeta'f(\frac{L}{X_w})$

$$P_{ij}=-\overline{u_iu_k}\frac{\partial U_j}{\partial x_k}-\overline{u_ju_k}\frac{\partial U_i}{\partial x_k},\qquad D_{ij}=-\overline{u_iu_k}\frac{\partial U_k}{\partial x_j}-\overline{u_ju_k}\frac{\partial U_k}{\partial x_i}.$$

Table 2: Constants in the pressure-strain correlation term

c_1^*	c_2^*	ζ^*	c_1'	c_2'	ζ'
1.4	0.44	-0.16	-0.35	0.12	-0.1

In the above equation, ζ is an independent constant to be determined from experimental data and α and β are to be defined as functions of c_2. On the other hand, in Launder, Reece and Rodi model, ζ, α and β are defined as functions of c_2 only. Therefore, the present model can take into account more experimental data than Launder, Reece and Rodi's model does.

The wall effect term $\pi_{ij,w}$ on turbulent stresses is included in this model by considering the empirical constants as the function of the dimensionless distance from the wall:

$$\left.\begin{aligned} c_1 &= c_1^*+c_1'f(L/X_w)\\ c_2 &= c_2^*+c_2'f(L/X_w)\\ \zeta &= \zeta^*+\zeta'f(L/X_w),\end{aligned}\right\} \tag{10}$$

$$f\left(\frac{L}{X_w}\right)=\frac{C_\mu^{3/4}k^{3/2}}{\kappa\varepsilon}\frac{1}{X_w}, \tag{11}$$

where $f(L/X_w)$ is the function of the dimensionless wall distance, and C_μ and k represent the empirical constant and the von Karman constant, respectively. It expresses the influence of the wall, takes the value of 1 in its vicinity, and approaches 0 with the increase of the distance. Here, X_w expresses the distance from the wall and L is defined as the length scale of turbulence. The values of these constants have been chosen such that, when $f=0$, the model yields the correct Reynolds stress components for nearly homogeneous shear flow of Champangne, Harris and Corrsin [17], and, when $f=1$, the relative magnitude of the stress components agrees with common consensus concerning to near-wall turbulence. Moreover, we have used the experimental data of Harris, Graham and Corrsin [18] who reported further homogeneous shear flow data where the strain rate is higher than Champagne, Harris and Corrsin's case. The pressure-strain correlation terms and constants used in this analysis are summarized in the Tables 1 and 2, respectively.

The fourth term of (1) is the homogeneous part of dissipation. This term is modeled

commonly with the assumption of the isotropic motion for the dissipation, namely:

$$\varepsilon_{ij} = 2\nu \overline{\frac{\partial u_i}{\partial x_k} \frac{\partial u_j}{\partial x_k}} = \frac{2}{3}\delta_{ij}\varepsilon. \tag{12}$$

A boundary-fitted coordinate system was introduced for this calculation. This system consists of coordinate transformation from the analysis domain, which is on the physical level, to the calculation domain, which corresponds to the calculation level for solving the governing equations. Although setup of the boundary conditions and discretization of the governing equations are easy in such boundary fitted coordinate system, the transformed governing equations need complicated algorithm. In order to improve numerical stability and convergence, the orthogonal coordinate system is preferred, and the following Poisson equation is introduced for grid generation: (for example, see Mastin and Thompson [19])

$$\begin{aligned}
&\alpha_{11}x_{\xi\xi} + 2\alpha_{12}x_{\xi\eta} + 2\alpha_{13}x_{\xi\zeta} + \alpha_{22}x_{\eta\eta} + 2\alpha_{23}x_{\eta\zeta} + \alpha_{33}x_{\zeta\zeta} \\
&\qquad + J^2\left[Px_\xi + Qx_\eta + Rx_\zeta\right] = 0, \\
&\alpha_{11}y_{\xi\xi} + 2\alpha_{12}y_{\xi\eta} + 2\alpha_{13}y_{\xi\zeta} + \alpha_{22}y_{\eta\eta} + 2\alpha_{23}y_{\eta\zeta} + \alpha_{33}y_{\zeta\zeta} \\
&\qquad + J^2\left[Py_\xi + Qy_\eta + Ry_\zeta\right] = 0, \\
&\alpha_{11}z_{\xi\xi} + 2\alpha_{12}z_{\xi\eta} + 2\alpha_{13}z_{\xi\zeta} + \alpha_{22}z_{\eta\eta} + 2\alpha_{23}z_{\eta\zeta} + \alpha_{33}z_{\zeta\zeta} \\
&\qquad + J^2\left[Pz_\xi + Qz_\eta + Rz_\zeta\right] = 0.
\end{aligned} \tag{13}$$

Here,

$$\alpha_{jk} = \sum_{m=1}^{3} \beta_{mj}\beta_{mk}, \tag{14}$$

$$M = \begin{bmatrix} x_\xi & x_\eta & x_\zeta \\ y_\xi & y_\eta & y_\zeta \\ z_\xi & z_\eta & z_\zeta \end{bmatrix}, \tag{15}$$

and ξ, η and ζ in the above equation are the transformed coordinate axes on the calculation level; P, Q and R are the parameters which control the spacing between the mesh points, respectively, and β_{jk} is defined as the cofactor in the matrix M. Each of the subscripts ξ, η and ζ indicates partial differentiation with respect to the corresponding coordinate direction.

The transformation of the governing equations to the calculation level is accomplished according to the following mathematical definitions:

$$\frac{\partial}{\partial x_i} = \frac{\partial \xi}{\partial x_i}\frac{\partial}{\partial \xi} + \frac{\partial \eta}{\partial x_i}\frac{\partial}{\partial \eta} + \frac{\partial \zeta}{\partial x_i}\frac{\partial}{\partial \zeta}. \tag{16}$$

For example, the momentum equation is transformed into the form including the Reynolds stress component as:

$$\frac{\mathrm{D}U_i}{\mathrm{D}t} = \frac{1}{\rho}\frac{\partial P}{\partial x_i} + \frac{\partial}{\partial x_j}\left(\nu\frac{\partial U_i}{\partial x_j} - \overline{u_i u_j}\right). \tag{17}$$

The Reynolds stress in the equation is divided into the term containing the velocity gradient and the remaining term.

$$-\overline{u_i u_j} = \left(\frac{b}{a}\right)_{ij} \frac{\partial U_i}{\partial x_j} - \left(\frac{c}{a}\right)_{ij}. \tag{18}$$

Here, the Reynolds stress is included as a part of the diffusion term and in order to improve the stability of the solution, we put:

$$d_{ij} = \nu + \left(\frac{b}{a}\right)_{ij}, \qquad e_{ij} = \left(\frac{c}{a}\right)_{ij}, \tag{19}$$

so that the equation of momentum can be rewritten in the following form:

$$\frac{\partial U_i}{\partial t} + \frac{\partial U_i U_j}{\partial x_j} = -\frac{1}{\rho}\frac{\partial P}{\partial x_i} + \frac{\partial}{\partial x_j}\left(d_{ij}\frac{\partial U_i}{\partial x_j} - e_{ij}\right). \tag{20}$$

Applying this formula to (16), it is finally transformed into:

$$\begin{aligned}
&\frac{\partial U_i}{\partial t} + \frac{\partial}{\partial \xi}\left\{\boldsymbol{U}U_i + \frac{P}{\rho}\xi_{xi} - \ell_1 U_{i\xi} - \ell_2 U_{i\eta} - \ell_3 U_{i\zeta} + \xi_x e_{i3} + \xi_y e_{i2} + \xi_z e_{i1}\right\} \\
&+ \frac{\partial}{\partial \eta}\left\{\boldsymbol{V}U_i + \frac{P}{\rho}\xi_{xi} - \ell_2 U_{i\xi} - \ell_4 U_{i\eta} - \ell_5 U_{i\zeta} + \eta_x e_{i3} + \eta_y e_{i2} + \eta_z e_{i1}\right\} \\
&+ \frac{\partial}{\partial \zeta}\left\{\boldsymbol{W}U_i + \frac{P}{\rho}\xi_{xi} - \ell_3 U_{i\xi} - \ell_5 U_{i\eta} - \ell_6 U_{i\zeta} + \zeta_x e_{i3} + \zeta_x e_{i2} + \zeta_z e_{i1}\right\} = 0,
\end{aligned} \tag{21}$$

$$\begin{aligned}
\ell_1 &= d_{i3}\xi_{x3}^2 + d_{i2}\xi_{x2}^2 + d_{i1}\xi_{x1}^2, \\
\ell_2 &= d_{i3}\xi_{x3}\eta_{x3} + d_{i2}\xi_{x2}\eta_{x2} + d_{i1}\xi_{x1}\eta_{x1}, \\
\ell_3 &= d_{i3}\xi_{x3}\zeta_{x3} + d_{i2}\xi_{x2}\zeta_{x2} + d_{i1}\xi_{x1}\zeta_{x1}, \\
\ell_4 &= d_{i3}\eta_{x3}^2 + d_{i2}\eta_{x2}^2 + d_{i1}\eta_{x1}^2, \\
\ell_5 &= d_{i3}\eta_{x3}\zeta_{x3} + d_{i2}\eta_{x2}\zeta_{x2} + d_{i1}\eta_{i1}\zeta_{x1}, \\
\ell_6 &= d_{i3}\zeta_{x3}^2 + d_{i2}\zeta_{x2}^2 + d_{i1}\zeta_{x1}^2,
\end{aligned} \tag{22}$$

$$\begin{aligned}
\boldsymbol{U} &= U_1\frac{\partial \xi}{\partial x_1} + U_2\frac{\partial \xi}{\partial x_2} + U_3\frac{\partial \xi}{\partial x_3}, \\
\boldsymbol{V} &= U_1\frac{\partial \eta}{\partial x_1} + U_2\frac{\partial \eta}{\partial x_2} + U_3\frac{\partial \eta}{\partial x_3}, \\
\boldsymbol{W} &= U_1\frac{\partial \zeta}{\partial x_1} + U_2\frac{\partial \zeta}{\partial x_2} + U_3\frac{\partial \zeta}{\partial x_3},
\end{aligned} \tag{23}$$

where $\boldsymbol{U}$, $\boldsymbol{V}$, $\boldsymbol{W}$ are the components of the contravariant velocity. The symbol of ℓ represents the metric tensor derived from the transformation.

In the case of three dimensional flows, the nine diffusion coefficients are needed. As for the other governing equations, application of the same steps leads to the transformed equations on the calculation level.

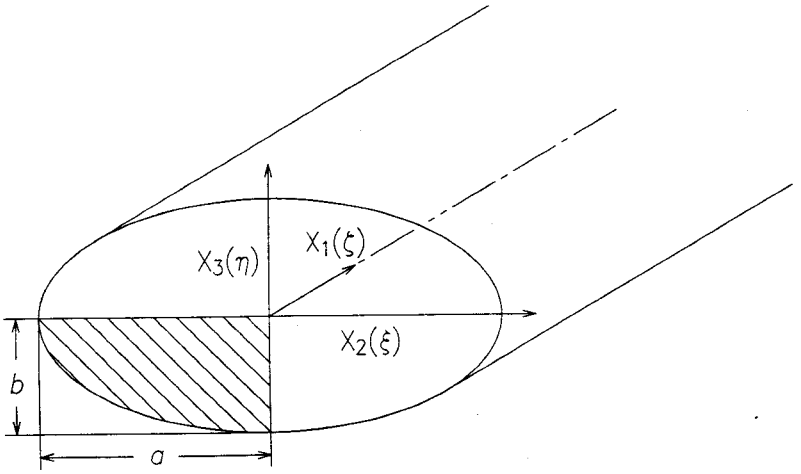

Fig.1: Coordinate system and calculation region

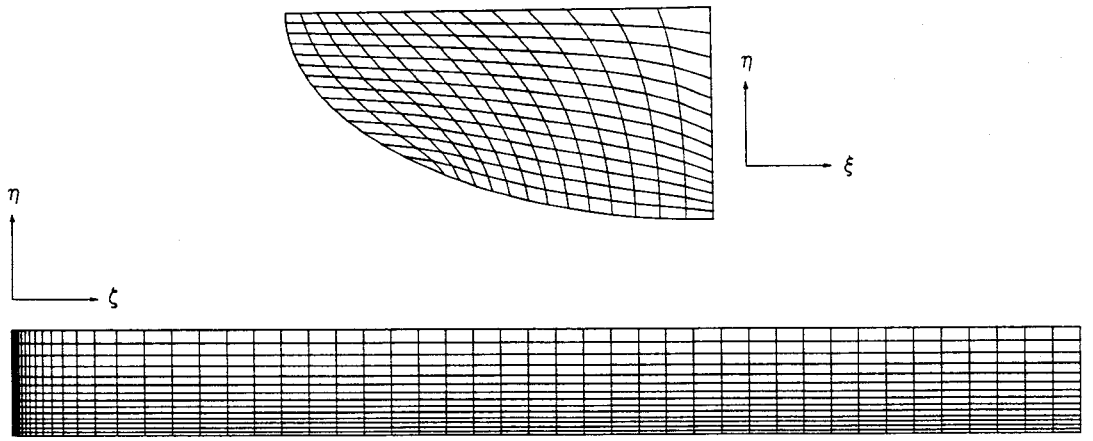

Fig.2: Calculation mesh

3. ANALYSIS RESULTS AND CONSIDERATIONS

Experimental works concerning turbulent flow in an elliptical duct are few. Cain and Duffy [9] showed the distributions of the average velocity and of the temperature. However, the characteristic quantities of turbulence were not presented. Their result is compared with the present calculations and, accordingly, the Reynolds number was set to 1.0×10^5. The length of the entrance section is chosen to be $97\,D_h$, where D_h represents the hydraulic diameter. For the analysis, the developing turbulent flows in an elliptical duct with the aspect ratio of 2:1 is considered.

Figure 1 shows the coordinate system used in the calculation. As seen in the figure, X_1 corresponds to the direction of the main flow, the axes X_2 and X_3 show the directions of the secondary flow. Object domain of the calculation is the region covered with shadow lines in Fig.1, which corresponds to 1/4 of the whole cross section based on consideration of the symmetry. Figure 2 shows the arrangement of the calculation mesh over the elliptical cross section. The mesh number is $(\xi\times\eta\times\zeta) = (15\times15\times50)$. The grid system of 15×15 for the

elliptical cross section was chosen to compare with the results calculated by Gosman and Rapley [10]. They calculated fully developed turbulent flow in elliptical cross section were using a grid system of 10×16, and reported that the solution are substantially independent of the mesh numbers if it is more than 250.

An isotropic turbulent flow with constant velocities is assumed at the inlet section. The turbulent energy k and dissipation ε are unknown from the experimental data, so that the values of $k = U_b \times 10^{-5}$, $\varepsilon = k^{3/2}/D_h$ were used as the inlet condition, which were chosen since the calculated results of developing turbulent flows in a square duct were proved to be in relatively good agreement with the experimental data reported by Melling and Whitelaw [3]. The Neumann condition is applied at the outlet section. As for the boundary conditions for the k and ε, the consistence of the universal velocity distribution at the vicinity of the wall and also the supposition of the local equilibrium lead to the utilization of the law of the wall function.

Concerning discretization of the governing equation, the QUICK scheme was used for the convection and diffusion terms and the central differential scheme was applied for other terms. In order to examine the validity of the present turbulent model and numerical scheme, we tested them on the developing turbulent flow in a square duct, which is experimented by Melling and Whitelaw [3]. As the result of this comparison, it is confirmed that the present method is able to predict the characteristic phenomenon for the developing flow in a square duct [13].

Figure 3 shows the distributions of the mean flow velocity calculated and those by the experiment along the axes X_2 and X_3. The values of the mean flow velocity are normalized by the friction velocity U_τ and U_c which represents the center-line velocity. This experiment was made at the Reynolds number equal to 9.215×10^4. In both figures, a good agreement between the calculated and the experimental data is found, except a small region near the wall.

Figure 4 shows a comparison of the friction factors calculated and measured by Cain and Duffy [9]. They are calculated using the following formula:

$$f = \frac{D_h \left(-\dfrac{\partial P}{\partial x_1} \right)}{\rho U_b^2/2}, \tag{24}$$

where P and U_b represent the pressure and the bulk velocity, respectively. The calculated friction factor is $f = 5.202 \times 10^{-3}$, which is only slightly higher than the observed value of $f = 4.983 \times 10^{-3}$ at the corresponding Reynolds number. Both of the calculated and the experimental data indicate higher value than the circular friction factor derived from Prandtl's universal law of friction.

Comparisons of the center-line mean velocity and the axial turbulent intensity are shown in Fig.5, in which a local maximum of the axial center-line velocity is observed. This is due merging of the shear layer with the boundary layer developing along the duct wall. This tendency is also observable during the build-up of the turbulent energy, although it is very small.

Figure 6 shows the mean flow velocity isolines at a section of $84.5\,D_h$ where the flow developed completely already and the turbulent energy isolines at the same location. Both of these values are normalized by the inlet velocity U_{in}. For $X_2/a = -0.66$, a warp is recognizable about the wall vicinity. This may be attributed to abnormal grid mesh around this position, as shown in Fig.2. Distortions of the 1.0 isoline of the velocity in the main flow direction and

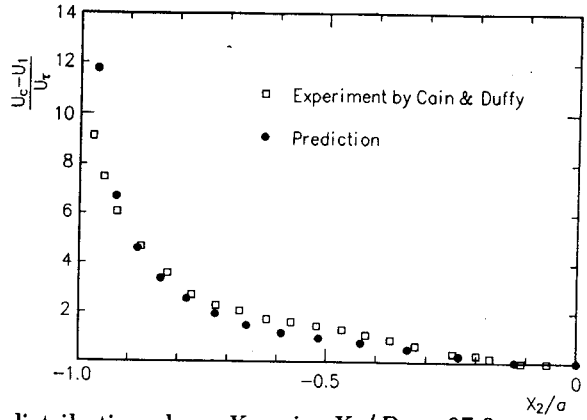

(a) Velocity distribution along X_2 axis: $X_1/D_h = 97.0$

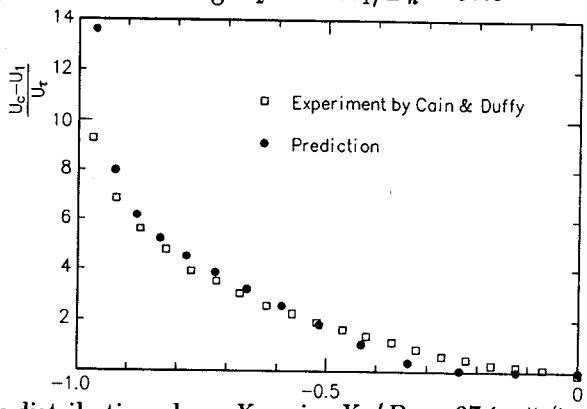

(b) Velocity distribution along X_3 axis: $X_1/D_h = 97.0$

Fig.3: Comparison of the velocities in the main flow direction

of 0.7 and 0.8 isolines of the turbulent energy are noticed. This trend is particularly clear for the isolines of the turbulent energy and strongly suggests the existence of the secondary flow of the second kind, which is peculiar phenomenon to the non-circular duct flow.

Figure 7 presents the velocity vector diagram showing the secondary flow of the second kind at a section of $84.5\,D_h$. Near the wall vicinity, a peak velocity up to about one percent of the main flow velocity is observed due to the secondary flow. For ducts with square and triangular cross sections, a pair of eddies is formed in each corner the domain, but only one eddy is formed for the elliptical duct with an aspect ratio of 2:1.

Nextly, the distributions of $(\overline{u_2^2} - \overline{u_3^2})$ and $\overline{u_2 u_3}$ are examined, which induce the secondary flow of the second kind. For fully developed flow, the equation of the streamwise vorticity ω_1 has the following form (in the coordinate system given in Fig.1):

$$U_2\frac{\partial \omega_1}{\partial x_2} + U_3\frac{\partial \omega_1}{\partial x_3} = \nu\left(\frac{\partial^2 \omega_1}{\partial x_2^2} + \frac{\partial^2 \omega_1}{\partial x_3^2}\right) + \frac{\partial^2}{\partial x_2 \partial x_3}\left(\overline{u_2^2} - \overline{u_3^2}\right) - \left(\frac{\partial^2}{\partial x_2^2} - \frac{\partial^2}{\partial x_3^2}\right)\overline{u_2 u_3}, \quad (25)$$

$$\omega_1 = \frac{\partial U_3}{\partial x_2} - \frac{\partial U_2}{\partial x_3}. \quad (26)$$

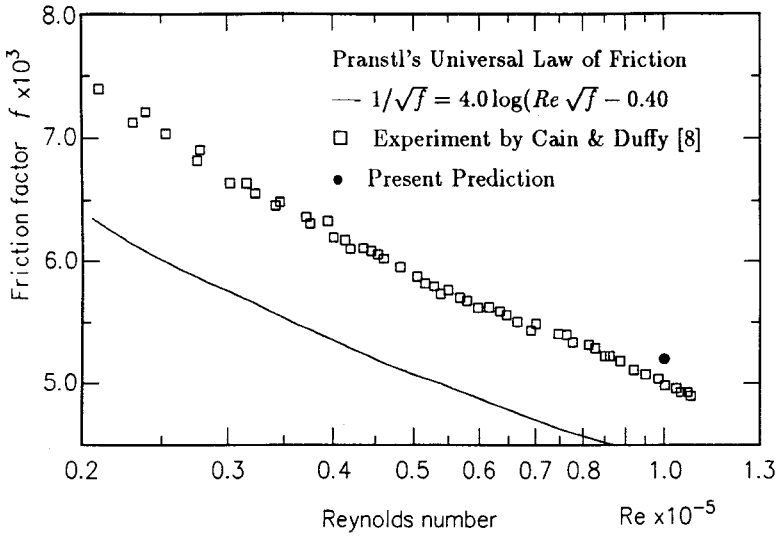

Fig.4: Comparison of the friction factor

The first term of the left hand side of (25) represents the convection of the streamwise vorticity due to the mean flow, and the first and second terms of the right hand side express the influence of the turbulent stresses on the production or destruction of the streamwise vorticity, and the third term is the damping due to viscosity. Judging from (25), the secondary flow of the second kind is induced due to the gradient of the difference of the normal stresses and the shear stress gradient. Therefore, in order to predict quantitatively the secondary flow, it is necessary to use anisotropic turbulence model in numerical analysis. Cain, Roberts and Barrow [20] have analyzed the momentum and energy equations for the fully developed turbulent flow with heat transfer in an elliptical duct. However, their method can not predict the secondary flow of the second kind since they applied the effective viscosity formulation for the turbulent model. Figure 8 shows the isolines of the normal stress difference $(\overline{u_2^2} - \overline{u_3^2})$ and the shear stress isolines $\overline{u_2 u_3}$.

The values of these parameters are normalized by the inlet velocity U_{in}. In the distribution of the normal stress difference, both of negative and positive regions exist. This pattern is also seen for the cases of the square and equilateral triangular ducts. On the other hand, the distribution of the shear stress $\overline{u_2 u_3}$ evolves with a comparatively high value at the vicinity of the wall from $X_2/a = -0.85$ to -0.58. In the cases of the square and equilateral triangular ducts, the shear stress develops along the diagonal line. From this point of view, the elliptical duct has quite different shear stress distribution from the non-circular duct with corner regions. In addition, the secondary flow of the second kind is comparatively stronger near the wall regions with high gradient values of the shear stress and the normal stresses difference. This result suggests that those quantities are contributing to generation of the secondary flow of the second kind.

Left of Fig. 9 shows the distribution of the shear stress $\overline{u_1 u_2}$. For the square and triangular ducts, it has been known that the distribution of $\overline{u_1 u_2}$ has a region with different sign in the

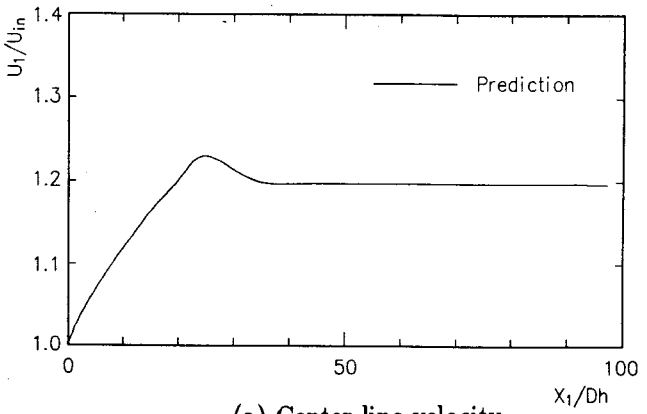

(a) Center-line velocity

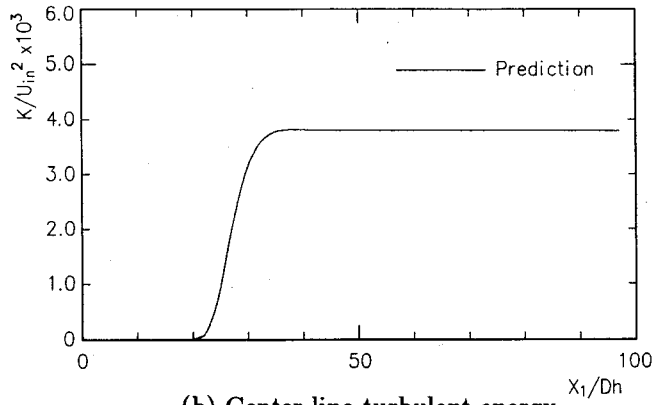

(b) Center-line turbulent energy

Fig.5: Axial variation of the center-line velocity and the turbulent energy

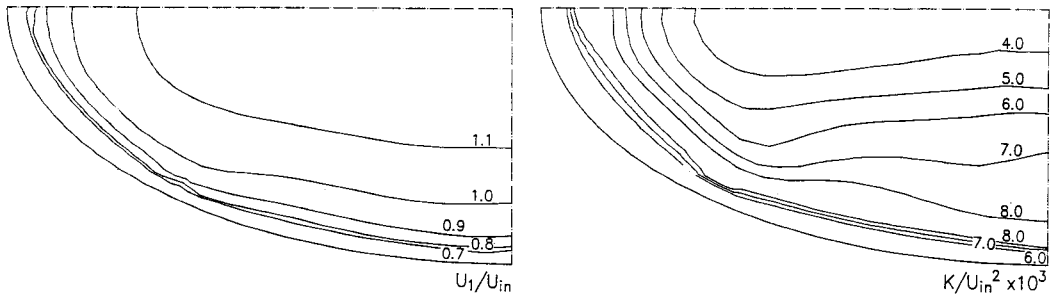

Fig.6: Contours of the mean flow velocity U_1/U_{in} (left) and the turbulent energy $k/U_{in} \times 10^{-3}$ (right)

vicinity of the left-right symmetry axis X_3. Melling and Whitelaw [3] pointed out that, in the developing flow of a square duct, two regions with the different signs of the shear stress $\overline{u_1 u_2}$ or $\overline{u_1 u_3}$ appear in the cross section as the flow develops. In the present results, a zero-line appears in the vicinity of the X_3 axis, and a small region with different sign can be recognized. Left and right of Fig.9 show the shear stress distribution at $X_1 = 84.5\, D_h$. Near the X_1 axis close to $25\, D_h$, where the interference of the boundary layers developed from the entrance takes place,

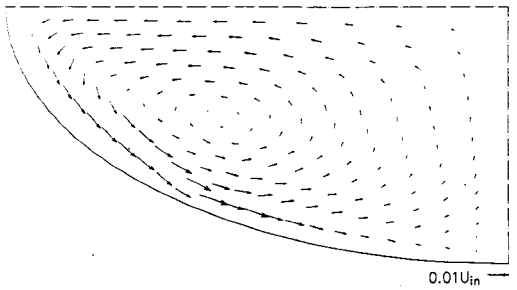

Fig.7:
Vector diagram of the secondary flow of the second kind

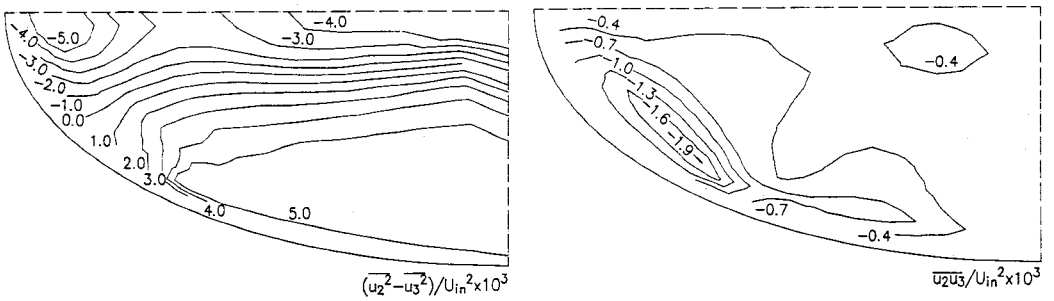

Fig.8 Contours of $(\overline{u_2^2} - \overline{u_3^2})/U_{in}^2 \times 10^3$ (left) and the shear stress $\overline{u_2 u_3}/U_{in}^2 \times 10^3$ (right)

this region becomes comparatively wide. Right of Fig.9 shows the distribution of the shear stress $\overline{u_1 u_3}$. The shear stress $\overline{u_1 u_2}$ develops along the X_2 axis and has high values in the wall vicinity. Contrary to this, the shear stress $\overline{u_1 u_3}$ develops along the X_3 axis and shows high value near the wall.

Figure 10 shows the velocity vector of the secondary flow of the second kind and the isolines of the secondary velocity component U_2 and U_3 at three different positions in the developing region. From these calculated results, it is seen that the value of the secondary flow reaches the maximum intensity at about 22.0 D_h which coincide with the position of the local peaking of the center-line mean velocity, as seen in Fig.5. This characteristic phenomenon was also observed for the calculated, developing turbulent flow in a triangular duct [13]. Therefore, the secondary flow has the maximum value on the way of the entrance region of the developing turbulent flow in the non-circular cross section.

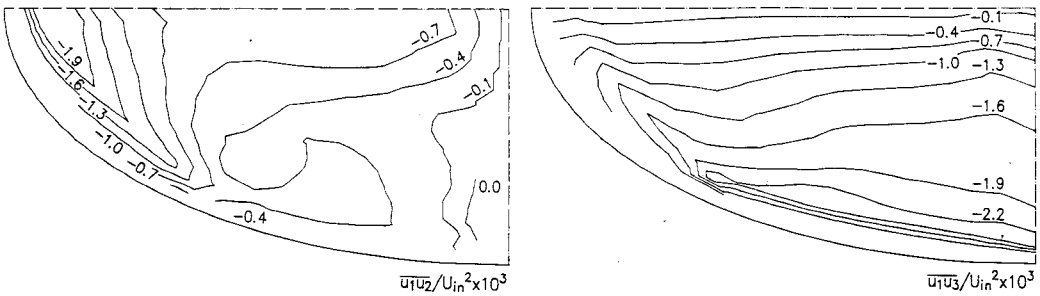

Fig.9: Contours of the shear stress $\overline{u_1 u_2}/U_{in}^2 \times 10^3$ (left) and $\overline{u_1 u_3}/U_{in}^2 \times 10^3$ (right)

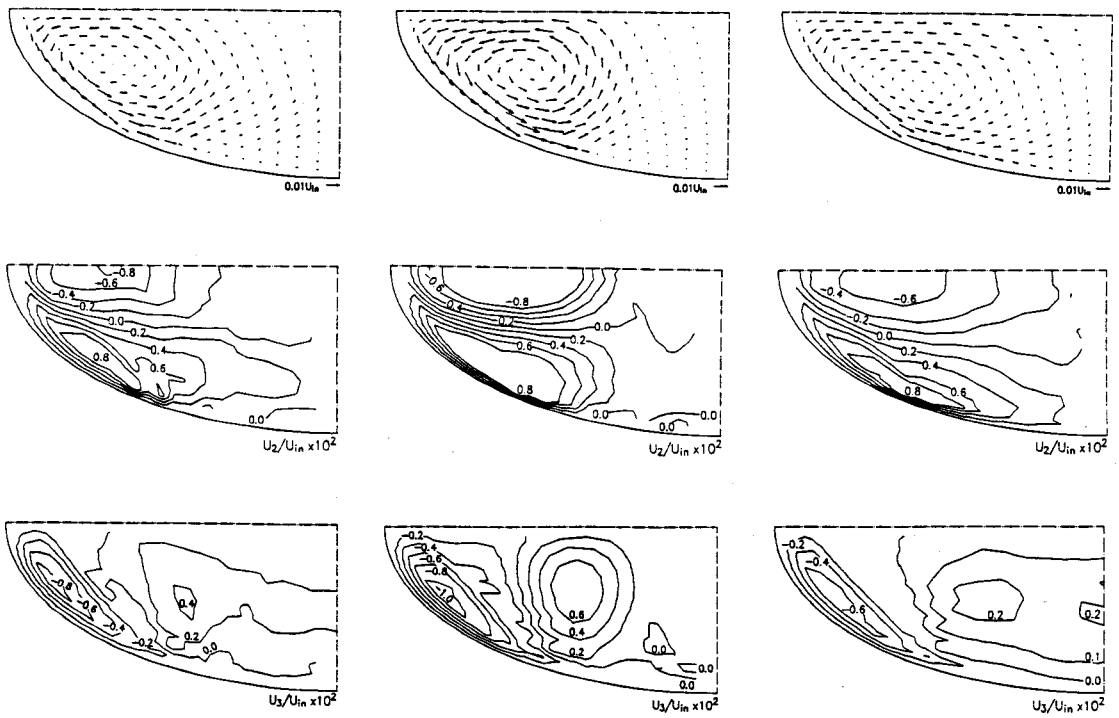

Fig.10: Predicted results of the secondary flow of the second kind in developing turbulent flow : $X_1 = 9.5\,D_h$ (left column); $X_1 = 22.0\,D_h$ (center column); $X_1 = 84.5\,D_h$ (right column); step $0.01\,U_{in}$ (top row); unit $U_2/U_{in}\times 10^2$ (middle row); unit $U_3/U_{in}\times 10^2$ (bottom row)

4. CONCLUSIONS

Numerical analysis of the developing turbulent flow in an elliptical duct has been carried out applying an algebraic stress model and a boundary-fitted coordinate system. The results of this analysis revealed the existence of the secondary flow of the second kind which is characteristic to non-circular duct flows. At the same time, a clear statement of the distributions of the various Reynolds stresses was made, showing their characteristic aspects. The distribution of the shear stress $\overline{u_2 u_3}$ over the directions of the secondary flow is found to be different from those reported for a duct with square or triangular cross section. For the latter cases, it has been known that, in the vicinity of the left-right symmetry axis, the distribution of $\overline{u_1 u_2}$ has a region with different sign. In the calculated case, a small region with different sign is also recognized. The secondary flow of the second kind reaches the maximum intensity in the middle of the developing stage. That is a result of merging of the shear layer with the boundary layer developing along the wall of the elliptical duct.

REFERENCES

[1] J.Nikuradse (1926) *Untersuchung über die Geschwindigkeitsverteilung in turbulenten Strömungen*; VDI–Verlage, Berline SW19

[2] E.Brundrett and W.D.Baines (1964) The production and diffusion of vorticity in duct flow; J. Fluid Mech., vol.19 pp.375-394

[3] A.Melling and J.H.Whitelaw (1976) Turbulent flow in rectangular duct; J. Fluid Mech., vol.78 pp.289-315

[4] R.E..Launder and W.M.Ying (1973) Prediction of flow and heat transfer in ducts of square cross-section; Heat and Fluid Flow, vol.3 pp.115-121

[5] F.B..Gessner and A.F.Emery (1976) A Reynolds stress model for turbulent corner flows: Part 1; Development of the model; J. Fluids Engineering, vol.98 pp.261-268

[6] H.J.Tracy (1965) Turbulent flow in a three-dimensional channel; J. Hydral. Div. A.S.C.E 91,(HY6) pp.9-35

[7] J.H.Leutheusser (1963) Turbulent flow in rectangular ducts; J. Hydral. Div. A.S.C.E 89,(HY3) pp.1-19

[8] A.M.M.Aly, A.C.Trupp and A.D.Gerrard (1978) Measurements and prediction of fully developed turbulent flow in an equilateral triangular duct; J. Fluid Mech., vol.85 pp.57-83

[9] D.Cain and J.Duffy (1971) An experimental investigation of turbulent flow in elliptical ducts; Int. J. Mech. Sci., vol 13 pp.451-459

[10] A.D.Gosman and C.W.Rapley (1978) A prediction method for fully developed flow through non-circular passages; Proc. Int. Conf. Numerical Methods, Paper No. FS/78

[11] T.Tatsumi and T.Yoshimura (1991) Instability of the rectangular duct flow and generation of the secondary flow; in: *Turbulence and Coherent Structures*; O.Métais and M.Lesieur, eds. Kluwer Acad. Publ.–1991

[12] H.Sugiyama, M.Akiyama and T.Serizawa (1991) Numerical analysis of developing flow in a square duct using Reynolds stress model; Proc. ASME/JSME Thermal Eng. Joint Conf. 1991, vol.3 pp.159-165

[13] H.Sugiyama, M.Akiyama, M.Hirata and S.Ueno (1990) Numerical solution of three dimensional turbulent flow in an equilateral triangular duct by Reynolds stress model; J. Comput. Fluid Dyn., vol.1 pp.104-114

[14] W.Rodi (1976) A new algebraic relation for calculating the Reynolds stresses; Z. Angew. Math. Mech., vol.56 pp.T219-T221

[15] P.Y..Chou (1945) On velocity correlations and the solutions of the equations of turbulent fluctuation; Quart. Appl. Math. vol.3 pp.38-54

[16] B.E.Launder, G.J.Reece and W.Rodi (1975) Progress in the development of a Reynolds stress turbulence closure; J. Fluid Mech., vol.68 pp.537-566

[17] F.H..Champagne, V.G.Harris and S.Corrsin (1970) Experiments on nearly homogeneous turbulent shear flow; J. Fluid Mech., vol.41 pp.81-139

[18] V.G.Harris, J.A.H.Graham and S.Corrsin (1977) Further experiments in nearly homogeneous turbulent shear flow; J. Fluid Mech., vol.81 pp.657-687

[19] C.W.Mastin and J.F.Thompson (1978) Transformation of three dimensional regions onto rectangular regions by elliptic systems; Number. Math., vol.29 pp.397-407

[20] D.Cain, A.Roberts and H.Barrow (1972) A theoretical study of fully developed flow and heat transfer in elliptical ducts; Proc. I. Mech. E. Conf. on Compact High Duty Heat Exchangers, pp.39-46